ORIGINAL PAPER

Experimental Investigation of Elastodynamic Nonlinear Response of Dry Intact, Fractured and Saturated Rock

Prabhakaran Manogharan[1] · Clay Wood[2] · Chris Marone[2] · Derek Elsworth[3] · Jacques Rivière[1] · Parisa Shokouhi[1]

Abstract

Nonlinear elastodynamic response of fractured rocks carries crucial information on fracture features that can be exploited to forecast flow properties, friction constitutive behavior and poromechanical response. Well-controlled laboratory experiments are designed to measure the nonlinear elastodynamic response of Westerly granite in three states: dry intact, dry fractured and saturated fractured. We study the effect of fracturing and saturation in modifying the elastodynamic response of the rock. Each sample is tested at a normal stress level of 15 MPa. We measure the elastodynamic response of an intact L-shaped sample of Westerly Granite subjected to normal stress oscillations of prescribed amplitudes (0.2–1 MPa) and frequencies (0.1, 1, 10 Hz). Ultrasonic waves transmitted across the sample are used to monitor the evolution of wave velocity before, during and after dynamic stressing. The nonlinearity of the elastodynamic response is measured in terms of: (1) the offset in normalized wave velocity; (2) the amplitude of wave velocity fluctuation during the oscillations; and (3) recovery rate of the wave velocity post-oscillation. We observe that the three nonlinearity parameters show a similar trend. Irrespective of the parameter, the nonlinearity measures higher for sample in dry-intact condition than that for dry-fractured and the saturated-fractured sample exhibits smaller nonlinearity than the dry-fractured sample. As expected, the saturated sample exhibits less nonlinearity than the dry intact and fractured samples due to the presence of interstitial fluid and the resulting increased interface stiffness. Conversely, the dry intact rock shows a higher nonlinearity than the dry fractured. We use numerical simulations to show that the presence of fracture significantly alters the strain distribution across the bulk of the sample and only the contacting asperities are highly strained, thus resulting in a decrease in the measured elastodynamic nonlinearity.

Keywords Nonlinear elastodynamic response · Rock fracture · Contact acoustic nonlinearity · Dynamic acousto-elastic testing

1 Introduction

Nonlinear elastic properties of fractured rock have important implications in managing engineered geothermal systems, waste storage, and unconventional reservoirs (Berkowitz 2002; Candela et al. 2015; Elkhoury et al. 2006, 2011). The nonlinear elastodynamic signatures of rock are rich in information on the microscopic characteristics of fracture interfaces, which also govern friction, fluid flow and seismicity (Bandis et al. 1983; Hudson et al. 1996; Pyrak-Nolte and Nolte 2016). Therefore, understanding the influence of fracturing and interstitial fluid on the elastodynamic response of rock is imperative in predicting its poromechanical properties (Acosta et al. 2020; Rutter and Mecklenburgh 2017, 2018). Even when macroscopically intact rocks exhibit strong elastic nonlinearity (Guyer and Johnson 2009), this nonlinearity is mainly due to their inherent heterogeneous microstructure. The nonlinearity of rocks manifests itself as strain-dependency in the elastic properties, hysteresis and slow dynamics (rate dependent and memory effects).

Earlier studies have reported on the nonlinear properties of rock using quasi-static analysis (Winkler and Liu 1996; Winkler and McGowan 2004). In quasi-static experiments, the sample is subjected to a gradual increase in the uniaxial stress or hydrostatic pressure, while changes in

✉ Parisa Shokouhi
  pxs990@psu.edu

1 Department of Engineering Science and Mechanics, The Pennsylvania State University, State College, USA

2 Department of Geosciences, The Pennsylvania State University, State College, USA

3 Energy and Mineral Engineering and Energy Institute, The Pennsylvania State University, State College, USA

the ultrasonic wave velocity are measured (acoustoelastic effect). The applied load is typically compressive to reflect natural in-situ conditions. Nonlinear behavior such as conditioning and slow dynamics are reported in experiments using resonance-based methods (Johnson et al. 1996; Remillieux et al. 2016; Rivière et al. 2015; Ten Cate and Shankland 1996; TenCate 2011; Van Den Abeele et al. 2000). More recently, dynamic acoustic-elastic testing (DAET) has been used in the laboratory to study the nonlinear elastodynamic behavior of rocks by measuring the strain-dependent variation in ultrasonic wave velocity and amplitude (Renaud et al. 2011, 2012, 2013a, b). Compared to resonance-based methods (Haupert et al. 2011; Johnson et al. 2009; Remillieux et al. 2016; Rivière et al. 2014; Van Den Abeele et al. 2000), which yield the average nonlinearity of the sample, DAET results are local and comprehensive (Lott et al. 2016; Renaud et al. 2016; Rivière et al. 2013). Another advantage of DAET is the resemblance of the experimental setup to field-scale processes (Johnson et al. 2009; Lawrence et al. 2008; Renaud et al. 2014). In DAET, the nonlinearity is characterized by measuring the change in ultrasonic wave velocity and/or amplitude before, during and after low-frequency perturbations (pump). Upon experiencing dynamic stress perturbation rocks exhibit a transient elastic softening inferred from the sudden drop in the ultrasonic wave velocity and amplitude. Following the perturbation, the wave velocity and amplitude slowly recover to the unperturbed state (slow dynamics). Field scale observations also show a decrease in seismic wave velocity in the vicinity of faults during an earthquake and subsequent recovery (Brenguier et al. 2008, 2014; Niu et al. 2008; Sens-Schönfelder and Eulenfeld 2019). This characteristic response (elastic softening and slow dynamics) is richly encoded with information on microstructures, fractures and contact mechanics.

Previous studies have reported smaller spectral amplitudes for naturally fractured specimens in comparison to intact specimens (equivalent to a lower transmission coefficient) and an upward shift in the peak frequency as the normal stress increases (Pyrak-Nolte et al. 1990). In addition, under saturated condition fluid present in fracture void spaces is found to increase the fracture specific stiffness (Pyrak-Nolte et al. 1990). Similarly, an increase in fracture stiffness with increasing confining pressure is also reported on artificial dry-fractured samples (Lubbe 2005). Both studies use quasi-static loading. Very recently, the influences of confining pressure and frequency on the nonlinear elastodynamic properties of dry rock are reported using DAET, but only intact samples are tested (Rivière et al. 2016). The influence of saturation on the nonlinearity of intact rocks is also studied using resonance-based methods (Johnson et al. 2004; Van Den Abeele 2002; Zinszner et al. 1997).

The effect of fracture under in-situ stress has not yet been studied. This study focuses on fractured rocks; in particular,

we use a DAET-like setup to investigate how fracturing alters the elastodynamic nonlinear response of a Westerly granite sample under in-situ stress conditions. Moreover, we report on the influence of saturation on the measured nonlinear elastodynamic response. While the nonlinearity of intact rocks arises from the distribution of soft grain boundaries and microcracks (Guyer and Johnson 2009; Rivière et al. 2015), the nonlinear elastodynamic response of fractured rock also includes the contact acoustic nonlinearity (CAN) due to the rough fractured interface. Our recent tightly controlled laboratory experiments suggest a coupling between the dynamic stiffness and permeability transients in fractured rock under true triaxial stress conditions (Shokouhi et al. 2020). A better understanding of the nonlinear elastodynamic behavior of fractured rock under in-situ stress is also essential in exploiting this coupling to predict the poromechanical properties of fractured rock.

2 Experimental Methods and Sample Preparation

Well-controlled laboratory experiments are conducted to measure the nonlinear elastodynamic response of Westerly granite under triaxial stress conditions in three states: (1) dry intact; (2) dry fractured; and (3) saturated fractured. A biaxial loading apparatus (Elkhoury et al. 2011; Samuelson et al. 2009) shown in Fig. 1a, is used to perform the experiments at 15 MPa normal stress loading conditions. The apparatus has two servo-controlled hydraulic pistons capable of applying vertical and horizontal loads in either displacement- or load-control modes, as shown in Fig. 1a. The horizontal piston is used to apply the normal loads in our experiments. The setup also includes a pressure vessel, as shown in Fig. 1a, to enable the application of confining pressure. All the stresses and pressures are recorded with a 10 V, 16-channel 24-bit analog-to-digital converter at a sampling rate of 10 kHz. Once the sample is loaded to the prescribed normal stress level (15 MPa), we actuate the horizontal piston to apply normal stress (low-frequency pump) oscillations of varying amplitudes (0.2–1 MPa) and frequencies (0.1–10 Hz). The horizontal piston is equipped with a load cell that measures the applied load to an accuracy of ± 5 N. A direct current displacement transducer (DCDT) (Trans-Tek Inc., series 240) is placed inside the pressure vessel to measure the horizontal displacement to an accuracy of ± 0.1 μm.

An L-shaped sample of dimension $68 \times 50 \times 45 \times 26$ mm is machined from Westerly granite rock, as shown in Fig. 1c. The sample is placed between steel loading blocks embedded with an array of piezoelectric transducers (PZTs, APC International Ltd, 6.5 mm in diameter), as shown in Fig. 1c. The sample is then placed inside the pressure vessel, as shown in Fig. 1b to carry out the experiments. Three
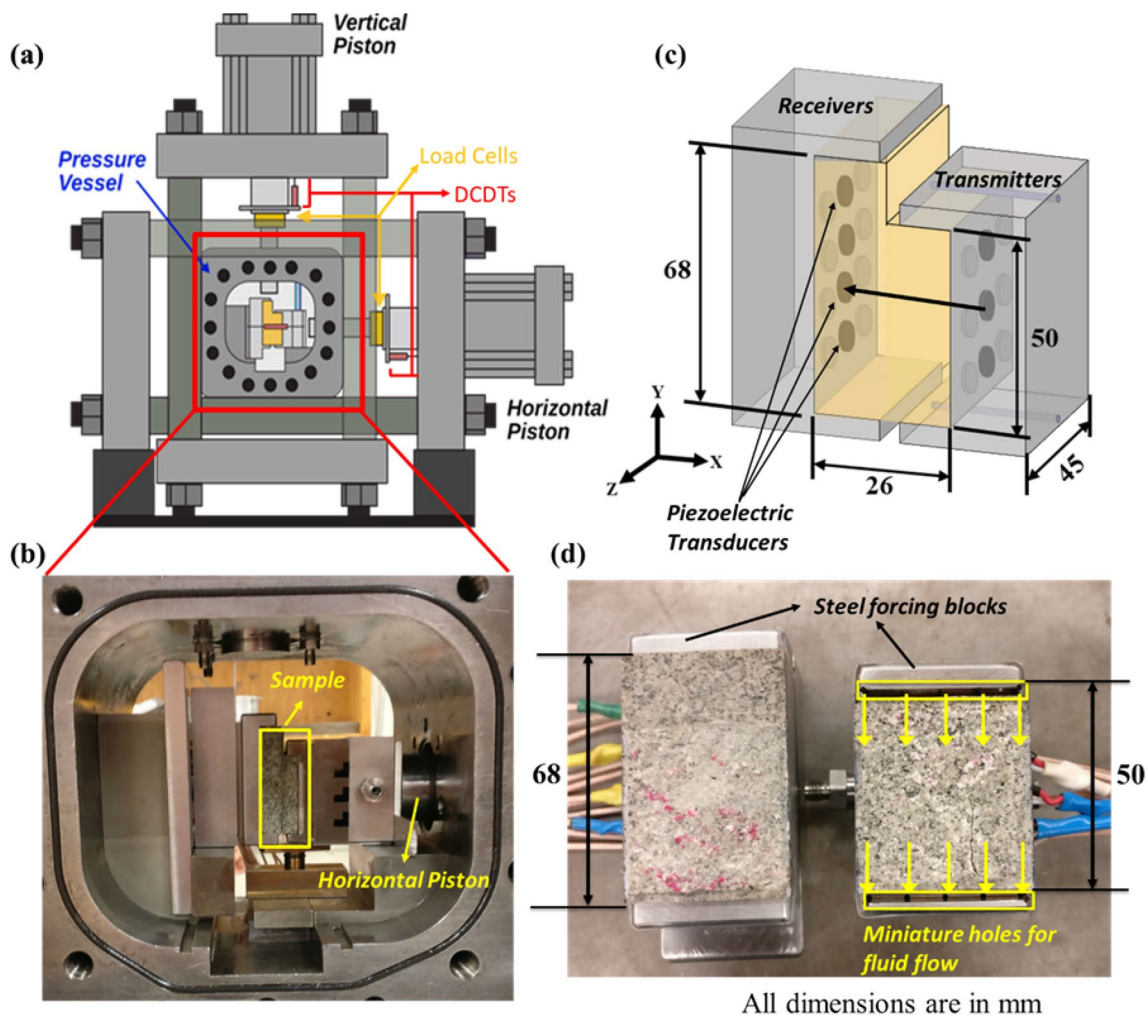
Fig. 1 **a** Schematic representation of the biaxial experimental setup; **b** Zoomed-in photograph of the sample assembly inside the pressure vessel; **c** L-shaped sample placed between the steel blocks with embedded ultrasonic transducers to probe the evolution of wave velocity before, after and during the dynamic oscillations. The activated transducers are marked in gray; **d** Photograph showing the two fractured halves secured between the steel forcing blocks which are then re-mated together to place inside the pressure vessel
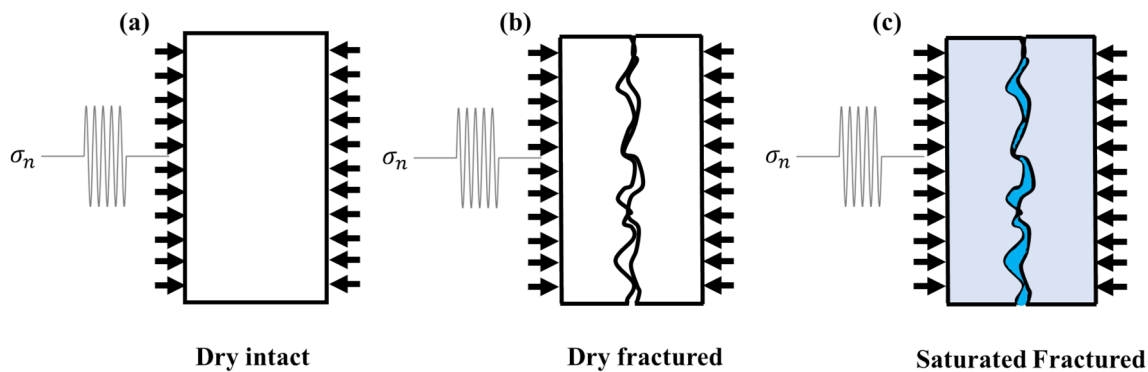

Fig. 2 Schematic representation of Westerly granite sample in three states: **a** Dry intact, **b** Dry fractured and **c** Saturated fracture

separate experiments are carried out on a single L-shaped sample under the three conditions, as shown in Fig. 2. The first experiment is on the dry intact sample. The second experiment is initiated by fracturing the dry sample outside the pressure vessel under tension. The two fractured halves are then re-mated along the fracture and placed between the steel loading blocks to perform the tests, as shown in Fig. 1d. During the intact and dry-fractured experiments, the doors of the pressure vessel are left open, as shown in Fig. 1b. Finally, we conducted a test on the fractured sample in the saturated condition. To saturate the fracture surfaces, we flow deionized and de-aired water across the fracture. The steel loading platens have miniature flow-distribution holes at the top and bottom (as shown in Fig. 1d) to allow flow across the fracture via a differential pore pressure ($(P_p)_{avg} = 1.6$ MPa). Due to the very low permeability of Westerly granite ($<10^{-20}$ m^2), it is reasonable to assume that the fracture is saturated, while the bulk of the sample is not. During the saturated test, the sample is completely sealed in a rubber jacket and enclosed in the pressure vessel under a confining pressure of 3.8 MPa. Flow across the fracture is controlled by upstream and downstream pore-pressure intensifiers—servo-controlled and fitted with an LVDT to measure volumetric flow rates. The average pore pressure is set such that the effective normal stress is similar to that for the dry experiments.

2.1 Dynamic Stress Protocol

Once the sample is loaded to the prescribed normal stress level (15 MPa), we impose normal stress oscillations of varying amplitudes (0.2–1 MPa) and frequencies (0.1, 1, 10 Hz), as shown in Fig. 3. The 0.4 MPa normal stress oscillation amplitude is repeated in between other amplitude oscillations, as shown in Fig. 3, to check the possible permanent changes in the fractured medium. A 90-s hold time is allocated between subsequent oscillations to allow recovery. A similar set of oscillation amplitudes is used for 1 Hz and 10 Hz frequency oscillations. In addition, we also repeat the 1 Hz oscillation amplitudes to check the reproducibility. Finally, the same oscillation protocol is used for all

three sample conditions to enable comparison among the elastodynamic responses.

2.2 Ultrasonic Data Analysis

A Vantage™ Research Ultrasound system (Verasonics®) is used to generate ultrasonic pulses and to record the response. As shown in Fig. 1c, piezoelectric crystals or PZTs (center frequency of 500 kHz) are embedded in the steel blocks 4 mm from the sample face to generate and receive ultrasonic pulses. PZTs are excited by a half sine wave pulse with a center frequency of 500 kHz (period $T = 2$ μs) with an amplitude of 96 V and pulse repetition frequency of 5 kHz. Out of the 9 transmitters and 12 receivers, only three transmitters and four receivers in the center array of each steel block are activated during the test (transmitters are arranged in the right block and receivers are arranged in the left block, as shown in Fig. 1c). We also note that due to the complexity of the experimental setup, limited space inside the pressure vessel and the harmful effect of the confining oil, some of the cables connecting the transducers inevitably fail during the experiments. For the dry-fractured sample we only have results for a single transducer pair due to failure of other transmitters. The results presented here pertain to T2–R2 pair for the dry-intact experiment and T3–R3 pair for the dry-fractured and saturated-fractured experiments (Fig. 4a).

Figure 5a, b shows the applied low frequency stress oscillation and the ultrasonic waves that are generated before and during the stress oscillation for a normal stress of 15 MPa. To measure the stress-induced change in wave velocity during the low frequency oscillation, the change in time (time shift) is calculated by cross correlation. We take a reference waveform during the unperturbed stress state. The reference waveform is then cross correlated with each subsequent ultrasonic wave pulses received during and after the low frequency oscillations. Here, signal 1 is the reference waveform obtained during the unperturbed stress state and signal 2 is taken during the low frequency stress oscillation, as shown in Fig. 5a, b. The window for the cross-correlation is selected carefully to include only the first p-wave arrival signal, as shown in Fig. 5c. The maximum of the cross-correlation function between the two signals gives the time

Fig. 3 Overview of the imposed normal stress oscillations on the sample for a 0.1 Hz frequency oscillation. The hold time between subsequent oscillations is 90 s
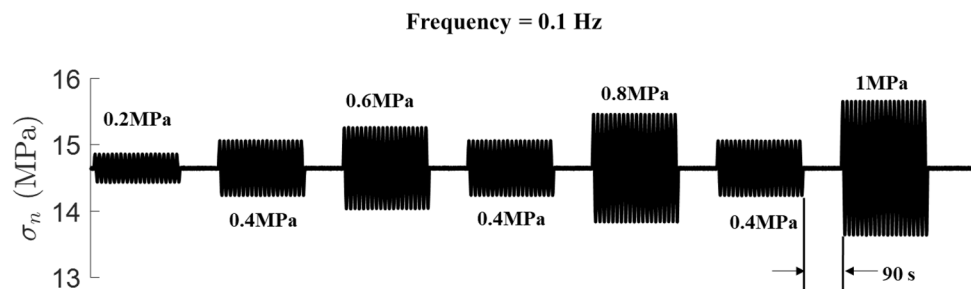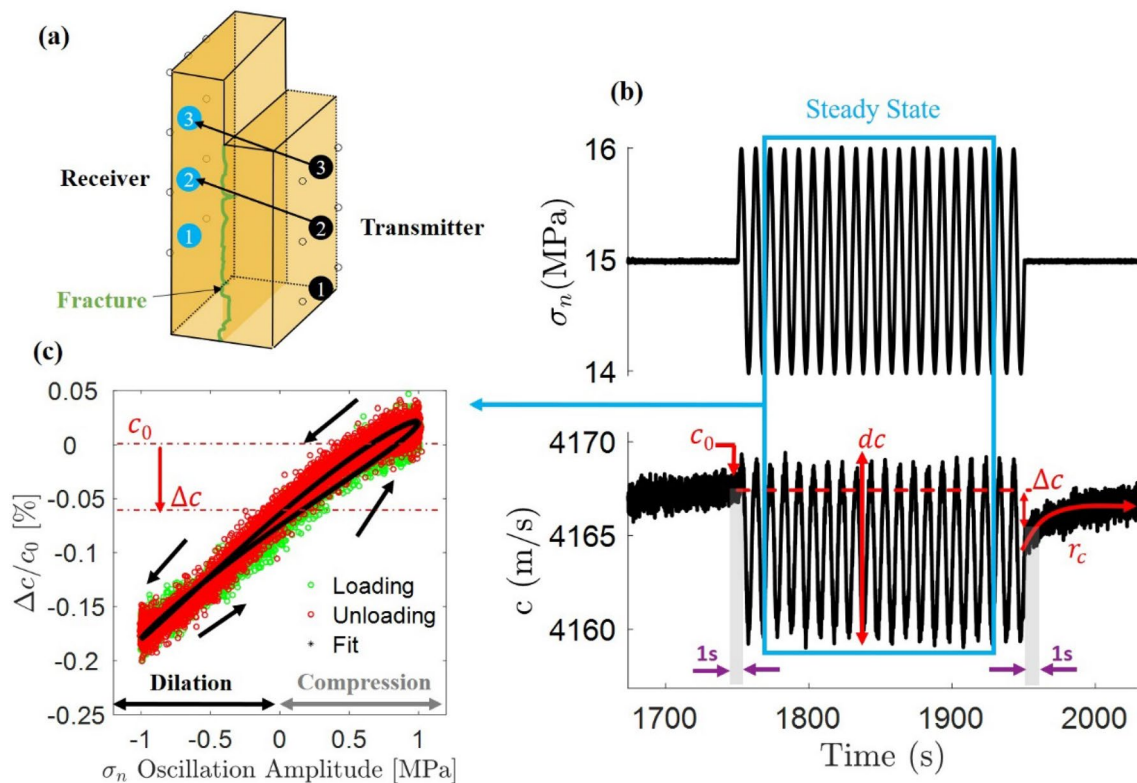
Fig. 4 a Schematic representation of the ultrasonic transmitter and receiver wave path across the fracture; **b** Example of the applied normal stress oscillation and the corresponding change in ultrasonic wave velocity for a 0.1 Hz-frequency oscillation. The drop-in wave velocity (Δc), pre-oscillation wave velocity c_0 averaged over a 1-s window, wave velocity amplitude change (dc) and the recovery of wave velocity (r_c) post oscillations are all marked; **c** Relative velocity change ($\Delta c/c_0$) vs. imposed stress during the non-equilibrium steady-state regime

shift value. Due to the second-order nature of the nonlinearity effects, the calculated time shift is very small, typically on the order of 1 ns, and smaller than the sampling time (40 ns). In other words, the sampling time resolution is not fine enough to allow us to estimate the time shift accurately. We use a second-order polynomial fit as a means of 'up-sampling' to improve the time shift estimation, as shown in Fig. 5d. The inset in the figure shows an example, where the cross-correlation peak is shown both with and without the polynomial fitting. The identified peak shifts from the red marker to the green marker, which improves the time-shift estimation. The measured time shift from all the ultrasonic waveforms with the reference waveform is shown in Fig. 5e. The wave velocity is then measured using the calculated and refined time shift, p-wave arrival time and the thickness of the sample without accounting for the small change in thickness due to loading. The displacement measurement shows that the change in thickness due to loading (including both static load and dynamic oscillation) is less than 23, 21 and 5 microns for dry-intact, dry-fractured and saturated-fractured experiment, respectively. The effect of such small thickness changes on the measured nonlinearity parameters is negligible.

3 Nonlinear Elastodynamic Response

We measure the ultrasonic response of the Westerly granite sample subjected to normal stress oscillations of prescribed amplitudes (0.2–1 MPa) and frequencies (0.1–10 Hz). The nonlinearity of each sample is evaluated by measuring the stress dependency of the wave velocity. Only three transmitters and three receivers are functional during this experimental series, and here, we only present the results pertaining to one transmitter–receiver pair for each sample condition (shown in Fig. 4a,). Fig. 4b represents a typical example of an applied normal stress oscillation and the corresponding changes in the ultrasonic wave velocity. Upon dynamic stressing, the wave velocity drops almost instantaneously (i.e., the rock sample suddenly softens) and oscillates at the frequency of stress oscillation and its higher harmonics, as shown in Fig. 4b. We measure the nonlinearity of the rock in terms of three parameters:
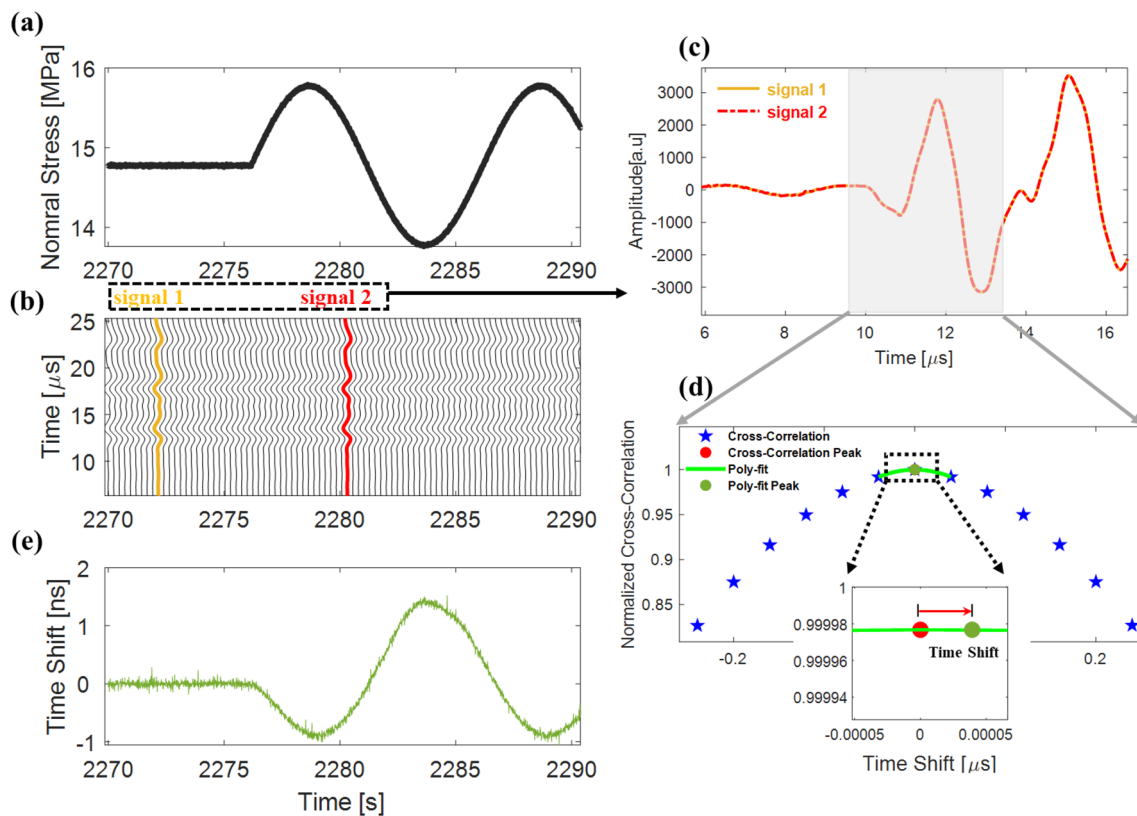

Fig. 5 Excerpt from saturated-fractured sample showing the procedure to calculate time shift. **a** Applied low-frequency normal stress oscillation. **b** Ultrasonic waveforms sent before and during the low frequency stress oscillation. **c** Reference waveform signal 1 taken during unperturbed stress state and signal 2 taken during the low frequency oscillation is shown for comparison. **d** Time shift is calculated by cross correlating the reference waveform signal 1 and signal 2. **e** Measured time shift from cross correlation of all the waveforms with the reference waveform

(1) the drop in wave velocity (Δc) due to dynamic stressing—sometimes referred to as *the offset*; (2) the average amplitude of the wave velocity fluctuations (dc) during the imposed oscillations (excluding 2 cycles at the beginning and at the end), which is related to the second harmonic content; and (3) the recovery rate of velocity (r_c) post oscillation, assuming a time-logarithmic trend (Shokouhi et al. 2017a, b; Ten Cate and Shankland 1996). The average amplitude of the wave velocity fluctuations or the second harmonic content of the wave velocity is measured using a projection procedure detailed in Rivière et al. (2013). To measure the recovery rate (r_c), we use the evolution of wave velocity over a 90-s data post the termination of each oscillation amplitudes, as shown in Fig. 45b. Both Δc and dc are normalized by the pre-oscillation wave velocity (c_0) averaged over a 1-s window preceding the oscillations, as illustrated in Fig. 4b. Figure 4c shows relative velocity changes ($\Delta c/c_0$) vs. normal stress during the steady-state regime marked in Fig. 4b.

4 Results

The nonlinear elastodynamic response of the sample is examined in three states (dry intact, dry fractured, and saturated fractured) and in terms of three nonlinear parameters (relative wave velocity change ($\Delta c/c_0$), average wave velocity amplitude change (dc/c_0) and wave velocity recovery rate (r_c). Specifically, we compare the response in these three states and demonstrate how the measured parameters change with normal stress oscillation amplitude and frequency. Figure 6 shows an example of how wave velocity changes with respect to the applied normal stress oscillations of varying amplitude and frequency under a normal stress 15 MPa for dry fractured sample. As mentioned earlier, the results presented here pertain to T2–R2 pair for the dry-intact experiment and T3–R3 pair for the dry-fractured and saturated-fractured experiments (refer to Fig. 4a).

Fig. 6 Excerpt from dry fractured sample wave velocity evolution due to normal stress oscillations of varying amplitude (0.2–1.0 MPa) and frequency (0.1 Hz, 1 Hz, 10 Hz) under a normal stress of 15 MPa. Inset shows the velocity for the various normal stress oscillation amplitudes for a frequency of 0.1 Hz
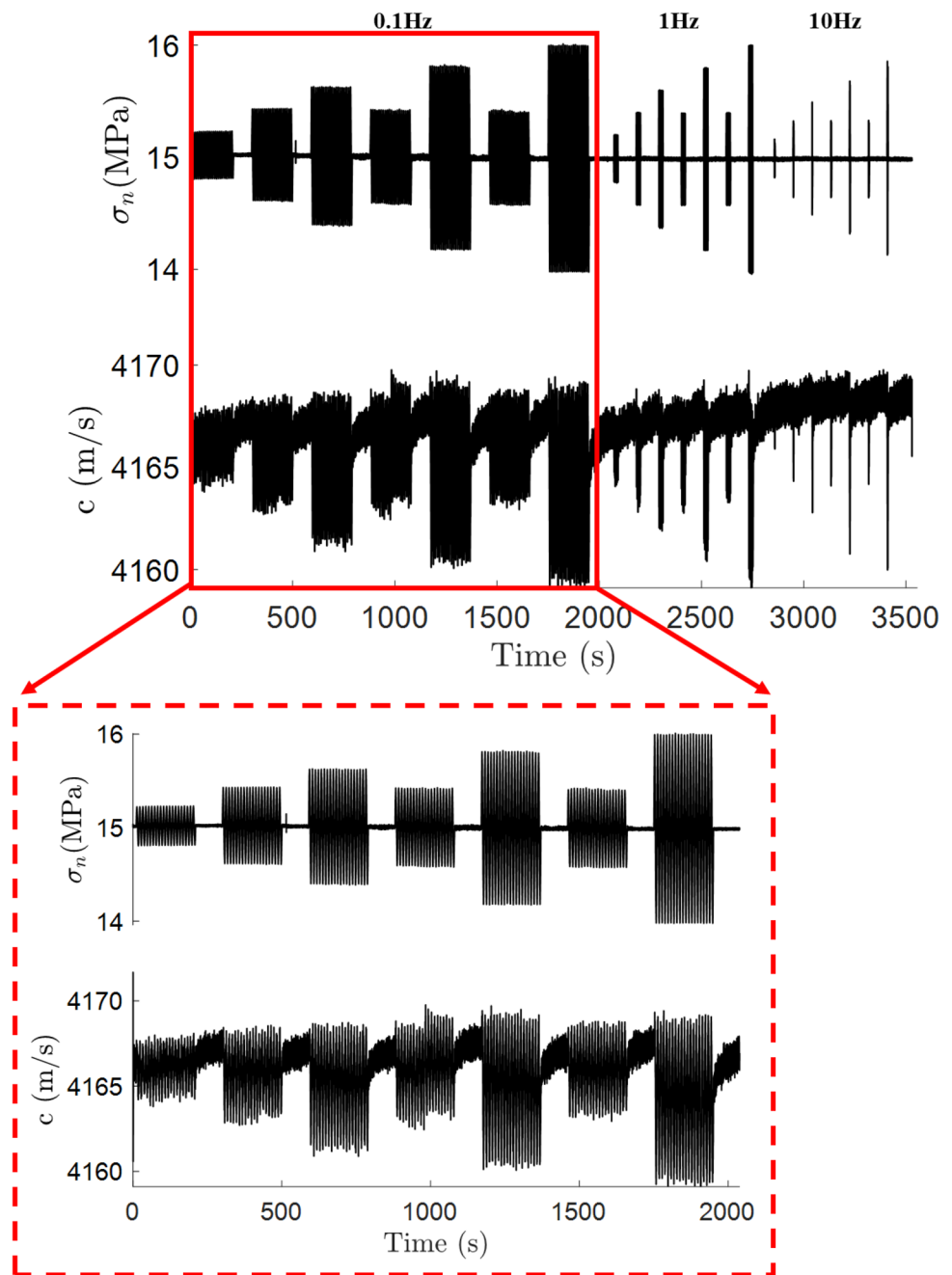
4.1 Amplitude- and Frequency-Dependency of $\Delta c / c_0$

The nonlinear parameter $\Delta c / c_0$ is plotted against the applied normal stress oscillation amplitude (0.2–1 MPa) in Fig. 7. The uncertainty in the measurement of $\Delta c / c_0$ (measured using the standard error of the mean Δc and c_0 during the 1-s window, as shown in Fig. 4b) is also plotted in Fig. 7 for all three-sample state, although not visible. The uncertainty in the measurement of $\Delta c / c_0$ is relatively small as shown in the inset of Fig. 7b. In addition, the repeated 1-Hz oscillation

shows the measurements are reproducible. Overlapping of the measurements corresponding to the three 0.4MPa oscillation amplitudes also confirms that there are no permanent damages in the system between the large oscillation amplitudes. The sample's response is more nonlinear if the absolute value of $\Delta c / c_0$ is larger at a given oscillation amplitude and frequency. As shown in Fig. 7a, $\Delta c / c_0$ of the intact sample increases as the normal stress amplitude increases. In addition, the nonlinearity seems to increase with the oscillation frequency. This trend closely resembles previous observations in dry intact Berea sandstone (Rivière et al. 2016).
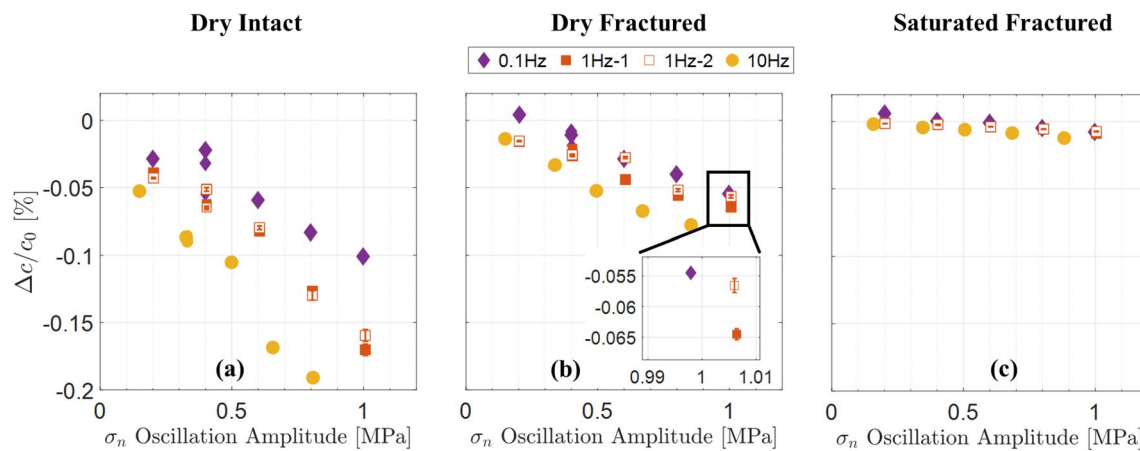
Fig. 7 Dependencies of relative velocity change $\Delta c/c_0$ on the amplitude and frequency of normal stress oscillations. **a** Dry intact; **b** Dry fractured and **c** Saturated-fractured samples. Note that because of the inefficiency of the loading system at higher frequencies, the applied normal stress oscillation amplitudes are slightly lower for the 10 Hz oscillation compared to other frequency oscillations

Similar trends are observed for the fractured sample in dry (Fig. 7b) and saturated (Fig. 7c) states. The results for the saturated-fractured sample at 1 Hz are also comparable to our previous observations on in-situ-stressed fractured samples of Westerly granite (Shokouhi et al. 2020). We observe that the saturated-fractured sample exhibits less nonlinearity than both the dry intact and fractured samples. For an intact sample, saturation decreases the pore compressibility, which increases wave velocity (Winkler and McGowan 2004) and decreases nonlinearity (Johnson et al. 2004; Ostrovsky and Johnson 2001). A decrease in the nonlinearity of an intact saturated rock sample has also been reported by Van den Abeele et al. (2002), Johnson et al. (2004) using a resonance-based method. For the saturated-fractured sample, the decrease in the measured nonlinearity is due to the presence

of the highly incompressible fluid and the resulting increased interface stiffness.

4.2 Amplitude- and Frequency-Dependency of dc/c_0

Figure 8 shows the normal stress amplitude- and frequency-dependency of the second extracted nonlinearity parameter dc/c_0 of the sample in the three states. The uncertainty in the measurement of dc/c_0 is also plotted in Fig. 8 for all three-sample state and it is relatively small. Similar to $\Delta c/c_0$, dc/c_0 scales linearly with amplitude although, the trend here is clearer. A linear dependency is also apparent in dry intact Berea sandstone (Rivière et al. 2015). In addition, there is no discernible dependency on the frequency of oscillations. This observation aligns with that reported
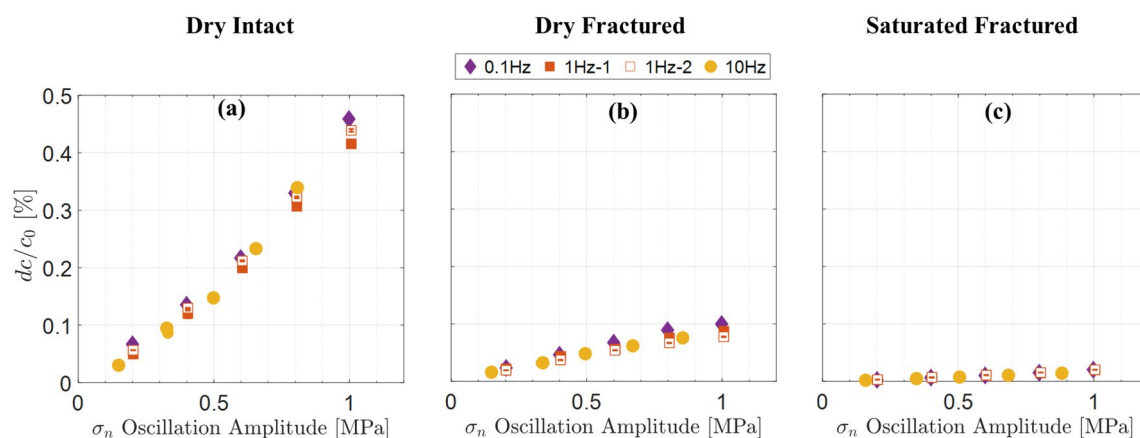

Fig. 8 Dependencies of average wave velocity amplitude change dc/c_0 on the amplitude and frequency of normal stress oscillations. **a** Dry intact; **b** Dry fractured and **c** Saturated-fractured samples

in a previous study (Rivière et al. 2016), where dc/c_0 or the second-harmonic amplitude is observed to be independent of the imposed oscillation frequency. Similar to what is observed for $\Delta c/c_0$, the dry intact sample's response shows more nonlinearity than the dry fractured sample, which in turn exhibits more nonlinearity than the saturated-fractured sample.

4.3 Recovery Rate

The recovery rate captures the late-time slow dynamic behavior of the three sample conditions. Following the dynamic perturbation, the wave velocity drops due to an
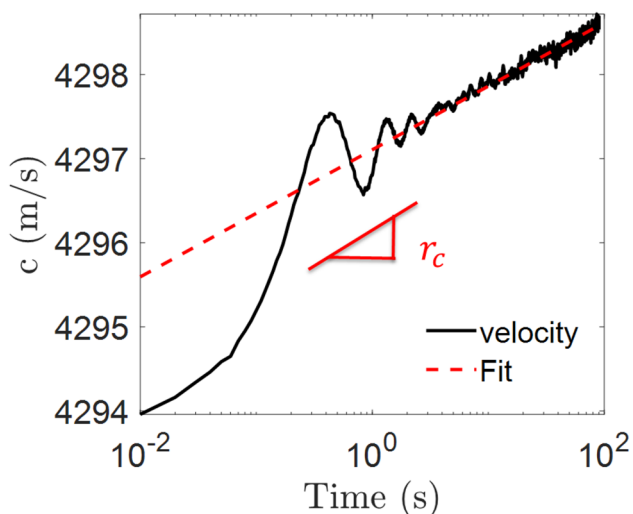

Fig. 9 Example showing the 90-s velocity data after the oscillation is used to fit the late time logarithmic trend by an equation of the form $c = r_c \log(t) + p$, where r_c and p are the slope (recovery rate) and intercept, respectively

instantaneous elastic softening, as shown in Fig. 4. Once the oscillation is removed, the wave velocity slowly increases towards the pre-oscillation value (c_0). The 90-s hold time between successive oscillations is sufficient for most of the relaxation to take place, although a full recovery may take significantly longer (Renaud et al. 2012). From a practical standpoint, waiting hours between oscillations to allow for full relaxation to take place is not feasible. Moreover, the focus of this paper is comparing the elastic nonlinearity in three different conditions rather than measuring the absolute nonlinearities. Since we maintain the same 90-s hold times for all sample conditions, such a comparison remains valid. In addition, we repeat 0.4 MPa oscillations in between larger amplitude oscillations. The almost overlapping $\Delta c/c_0$ values (see Fig. 7) are an indication that the influence of the irrecoverable changes (caused by not waiting long enough) on our measurements is insignificant. Regardless of the state, the wave velocity follows a time-logarithmic trend as illustrated in Fig. 9 for a dry fracture sample with 1 MPa-oscillation at 0.1 Hz. This observation is consistent with previous observations (Shokouhi et al. 2017a; Ten Cate and Shankland 1996), where a late-time time-logarithmic recovery is reported.

To measure the recovery rate, the late-time recovery of wave velocity is described by an equation of the form $c = r_c \log(t) + p$ shown as fit in Fig. 9, where r_c and p are the slope (recovery rate) and intercept, respectively. Figure 10 shows the amplitude- and frequency-dependency of the slope r_c. We observe that r_c increases with the normal stress oscillation amplitude and decreases with the frequency of oscillations. Of the three sample states, r_c is the largest for the dry intact sample and smallest for the saturated-fractured condition. This observation is consistent with that reported for the other two nonlinearity parameters discussed above. Moreover, this consistent observation further reinforces the
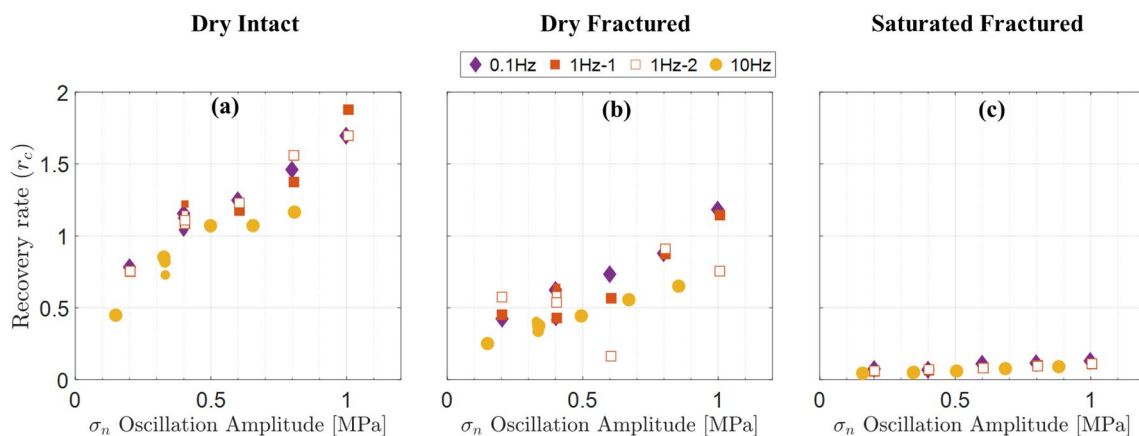

Fig. 10 Dependencies of log(t) recovery rate r_c on the amplitude and frequency of normal stress oscillations. **a** Dry intact; **b** Dry fractured and **c** Saturated-fractured samples

fact that although unknown, the physical mechanisms for conditioning or elastic softening (measured by $\Delta c/c_0$) and recovery or slow dynamics (measured by r_c) may be similar (i.e., opening and closing of microcracks, grain–grain contacts, soft inclusions) as reported by Johnson and Sutin (2005).

5 Discussion

Here we investigate the surprising result that dry-fractured sample exhibits higher nonlinearity than the dry-intact sample and propose a hypothesis for the observed behavior. We also investigate the effect of mating fractured surfaces and confining pressure/bounday condition on the measured nonlinear elastodynamic respose. Finally, we discuss the implications of our results in geophysical applications.

5.1 Dry-Intact vs. Dry-Fractured

The three nonliearity parameters $\Delta c/c_0$, dc/c_0 and r_c all behave in a similar fashion. Interestingly, the sample when dry and intact exhibits higher nonlinearity than when dry and fractured. This observation is surprising, since the presence of the fracture and associated contact acoustic nonlinearity (Jin et al. 2018, 2020) should result in greater nonlinearity. One hypothesis is that the presence of the fracture alters the strain distribution across the fractured sample such that the bulk of the sample remains insufficiently strained to exhibit nonlinearity—it is acoustically isolated. To test this hypothesis, we performed a 2D numerical simulation using COMSOL Multiphysics® version 5.4 (COMSOL 2019) to compare the strain distribution across an intact sample with that for a fully fractured sample, where a rough contact interface (sinusoidal in nature) presses against a flat surface of the same material (see Fig. 11). The thickness of

the sample is chosen to be similar to our actual sample size (26 mm). Young's modulus and Poisson's ratio are assumed to be 60 GPa and 0.6, respectively. The interaction between the contact surfaces is established by a surface-to-surface contact pair algorithm. The friction between the surfaces is controlled by the static coulomb friction model with a friction coefficient of 0.3. To simulate the exact experimental conditions, we follow a two-step analysis. Initially, a stationary (static) step is applied to simulate the normal load by applying a horizontal displacement (10 µm) uniformly on the right end of the model, as shown in Fig. 11. This produces a normal stress of 15 MPa in the sample. Second, a frequency-domain step is added to simulate the dynamic oscillation by applying a forced excitation on top of the displacement load, as shown in Fig. 11. Other boundary condition includes a fixed BC on the left end of the model. Figure 11 shows the strain in the x-direction for an intact and fractured sample for an oscillation frequency of 10 Hz. Comparing the strain fields in the models, we observe the uniform strain in the intact sample while the strain is non-uniformly distributed when fractured. Although the strain is higher in the fractured model, only the contacting asperities are highly strained while strain in bulk of the sample remains relatively low compared to intact model. This observation is similar irrespective of the applied frequency. To activate the nonlinearity of a medium the applied strain must be sufficiently high (Pasqualini et al. 2007; Guyer and Johnson 2009; Van Den Abeele 2007). In other words, the measured nonlinearity depends on the strain the sample experiences; the nonlinearity of the fractured sample is less than that for the intact sample, because the strain experienced by the bulk of the fractured sample is smaller than experienced by the intact sample. The strain distribution in the fractured sample depends on the fracture interface roughness including the size and distribution of asperities. Irrespective of the fracture roughness, we expect high stress concentrations on the

Fig. 11 2D Finite-element simulations comparing the axial strain distribution (ϵ_{xx}) of an intact sample and a rough fracture surface in contact with a flat surface

Total Strain Distribution (ϵ_{xx})
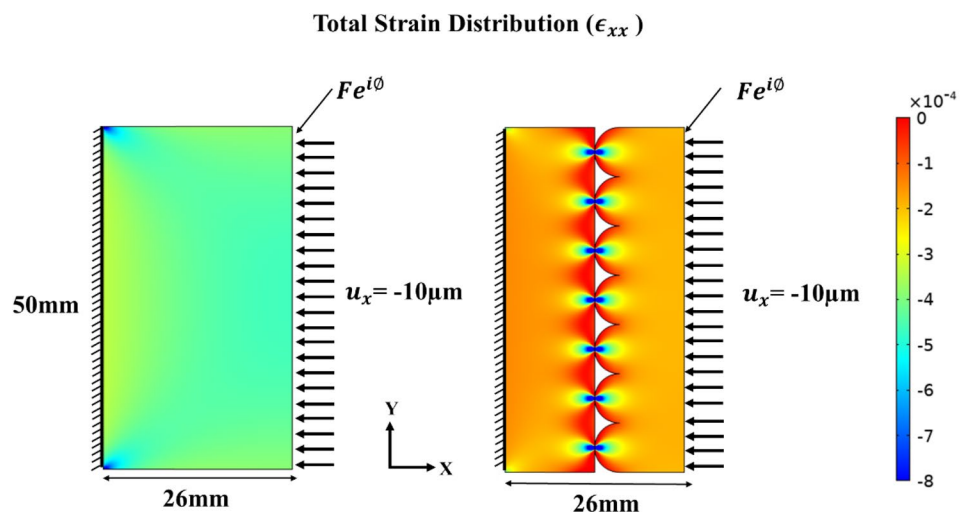
asperity contacts with the bulk of the sample experiencing less strain leading to a smaller measured nonlinearity than that measured for the intact sample.

5.2 Effect of Mating Fractured Surfaces

Our results show that the saturated-fractured sample is less nonlinear than the dry-fractured sample. Saturating the fractured surfaces with highly incompressible fluid increases the interface stiffness, which in turn decreases the measured nonlinearity. A possible source of variation between the measured nonlinearities for the specimen in dry-fractured and saturated-fractured conditions is differences in re-mating of the two fractured surfaces when conducting the two experiments. However, when we repeat the saturated-fractured experiment using the same sample, we observe that $\Delta c/c_0$ vs. normal stress oscillation amplitude is fairly similar between the two experiments, as shown in Fig. 12, comparing the results from the same transducer pairs. Importantly, nonlinearity measured in both experiments is significantly smaller than that measured in the dry-fractured condition. These results confirm that the effect of possible misalignment on the reported results is small.

5.3 Effect of Boundary Condition/Confining Pressure

Saturated-fractured experiment is conducted under a confining pressure of 3.8 MPa while keeping the effective normal stress at ~15 MPa and the sample completely sealed in a rubber jacket. However, the two dry experiments are conducted at a normal stress of 15 MPa at ambient pressure. In other words, the pressure boundary conditions are exactly the same for the sample in dry intact and fractured conditions, but it differs for the sample in saturated-fractured condition. We carried out an additional set of experiments to investigate the influence of varying boundary conditions

on the reported results for the sample in dry-fractured condition. The same fractured sample is re-mated, completely sealed in a rubber jacket and enclosed in the pressure vessel to simulate the similar boundary conditions to those in saturated-fractured experiment. The confining pressure (P_c) is increased from 0 to 3.8 MPa, 7 MPa and 10.3 MPa while maintaining the effective normal stress ($\sigma_{\text{eff}} = \sigma_N + 0.321 P_c$) constant at ~15 MPa. In this equation, 0.321 is the ratio of the surface area covered by the horizontal piston (pressed against the sample) and the remaining surface area of the sample uncovered by the piston. The dynamic stress oscillation protocol is similar to the one shown in Fig. 3, except that we only apply 1-Hz frequency oscillation of varying amplitudes.

Figure 13 shows the results obtained using two transducer pairs (T2–R2 and T3–R3, refer to Fig. 4a) when testing the fractured sample. Figure 13a illustrates that the relative velocity change $\Delta c/c_0$ vs. the applied normal stress oscillation amplitude measured for T3–R3 at $\sigma_N = 15$ MPa and $P_c = 0$ MPa is similar to the results reported in Fig. 7b for the same transducer pair (Note the scale difference between Fig. 7b and 13a). Besides small variations possibly due to re-mating of the fractured surfaces between the two experiments, the slight decrease in the $\Delta c/c_0$ in Fig. 13a compared to that shown in Fig. 7b may be attributed to the permanent changes in the fractured medium due to repeated experiments carried out on this sample. Importantly, the measurements at $\sigma_N = 13.5$ MPa and $P_c = 3.8$ MPa shown in Fig. 13b are similar to the results obtained at ambient pressure shown in Fig. 13a, although the data shows larger scatter. Increasing the confining pressure to 10.3 MPa does not appear to change $\Delta c/c_0$ (no data are available for $P_c = 7$ MPa). Considering the results corresponding to the other available transducer pair (T2–R2) shown in Fig. 13e–h, we do not observe much change in $\Delta c/c_0$ with increasing confining pressure except at $P_c = 10.3$ MPa, where a slight decrease is recorded. These observations suggest that the

Fig. 12 Relative velocity change $\Delta c/c_0$ vs. the applied normal stress oscillation amplitude for two saturated-fractured experiments conducted using the same fractured sample independently at two different times: **a** results reported previously in Fig. 7c, **b** results obtained on the same sample at a later time. The similarity of the two sets of results indicates that the variation due to the differences in re-mating of the fracture surfaces is small
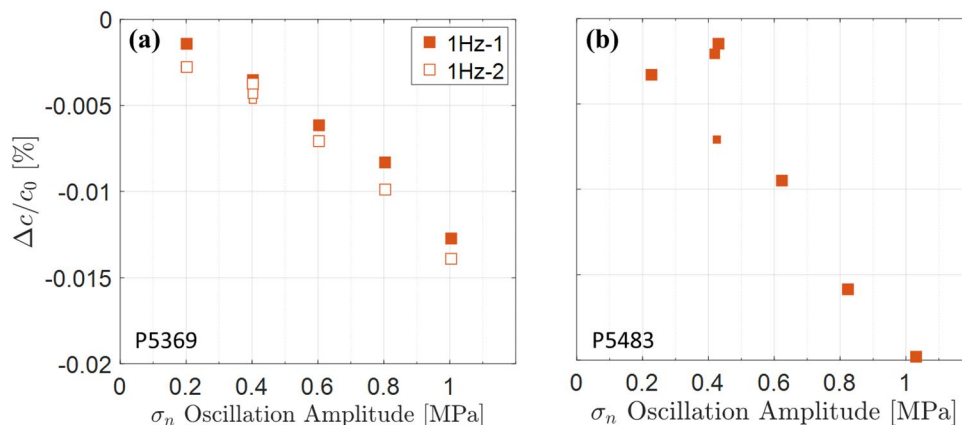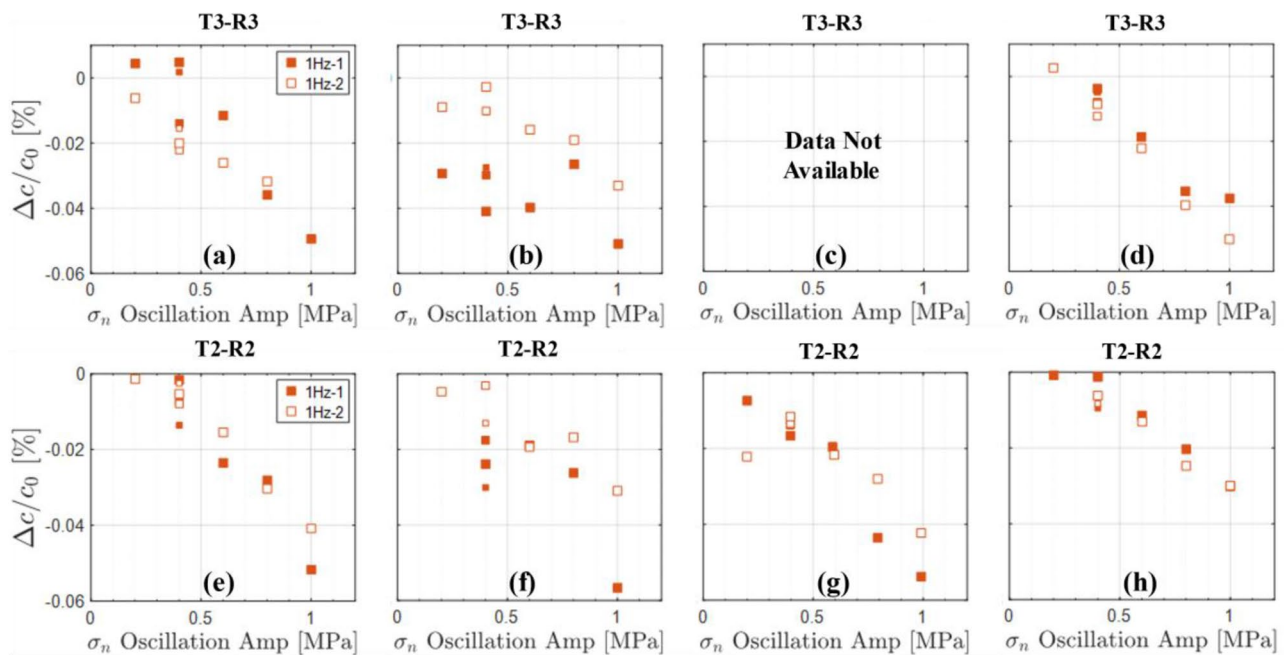
Fig. 13 Relative velocity change $\Delta c/c_0$ vs. the applied normal stress oscillation amplitude for the dry-fractured samples at varying combinations of confining pressure and normal stress. The confining pressure and normal stress are chosen, such that the *effective* normal stress is kept constant at ~15 MPa in all cases. The top row (**a–d**) corresponds to transducer pair T3–R3, while the bottom row (**e–h**) corresponds to T2–R2 pair. **a, e** σ_N = 15 MPa and P_c = 0 MPa; **b, f** σ_N = 13.5 MPa and P_c = 3.8 MPa; **c, g** σ_N = 12.3 MPa and P_c = 7 MPa; **d, h** σ_N = 11 MPa and P_c = 10.3 MPa

effect of confining pressure on the measured nonlinearity of dry-fractured sample is small and that the nonlinearity of the dry-fractured sample measures larger than that for saturated-fractured sample with the same boundary conditions.

5.4 Geophysical Prospection

The reported nonlinear elastodynamic response has implications in deep reservoirs, particularly near fractures or fault zones. An effective stress of 15 MPa in our experiment represents in-situ stress conditions at ~1 km depth below the surface. A study by Rivière et al. (2016) on dry-intact sandstone under varying confining pressure between 0.1 and 30 MPa has shown that the nonlinearity decreases by an order of magnitude as the pressure increases from 0 to 10 MPa and further decreases exponentially from 10 to 30 MPa. Although the microstructural mechanics at play is unclear, the decrease in nonlinearity is attributed to crack closure under high pressures. Further experiments are needed to determine whether the nonlinearity of a fractured sample continues to decrease or saturates under high stresses. Nevertheless, high elastic nonlinearity can still be observed in deep but fluid over-pressured zones, where the effective stress is typically low due to the presence of unusually high pore fluid pressure (Aminzadeh and Dasgupta 2013).

6 Conclusion

We report the nonlinear elastodynamic response of the Westerly granite rock in three conditions: dry intact, dry fractured and saturated fractured. The nonlinearity of each sample is evaluated by measuring the stress-dependency of wave velocity. The effect of fracturing and saturation in modifying the elastodynamic response is studied using three nonlinear parameters: wave velocity offset due to imposed normal stress oscillations, amplitude of wave velocity fluctuation during the oscillations and recovery rate of wave velocity post oscillations. The observations for all three nonlinear parameters are consistent. Our findings indicate that the saturated-fractured sample exhibits less nonlinearity than both the dry-intact and dry-fractured samples. In addition, the dry fractured sample appears less nonlinear than the dry-intact sample. The smaller measured nonlinearity for the fractured sample is attributed to a non-uniform strain distribution across the fractured sample such that bulk of the sample is not sufficiently strained to activate the nonlinearity.

Understanding the nonlinear elastodynamic response of fractured rock in different states offers the promise of illuminating the coupling between fracture stiffness and permeability transients and enabling remote and non-destructive characterization of these behaviors in situ. Our future experiments on saw-cut samples of uniform roughness will be used

References

Acosta M, Maye R, Violay M (2020) Hydraulic transport through calcite bearing faults with customized roughness: effects of normal and shear loading. J Geophys Res Solid Earth 125:1–29. https://doi.org/10.1029/2020JB019767

Aminzadeh F, Dasgupta SN (2013) Geophysics in drilling. In: Developments in Petroleum Science. Elsevier B.V., pp 223–246. https://doi.org/10.1016/B978-0-444-50662-7.00008-1

Bandis SC, Lumsden AC, Barton NR (1983) Fundamentals of rock joint deformation. Int J Rock Mech Min Sci Geomech Abstr 20:249–268. https://doi.org/10.1016/0148-9062(83)90595-8

Berkowitz B (2002) Characterizing flow and transport in fractured geological media: a review. Adv Water Resour 25:861–884. https://doi.org/10.1016/S0309-1708(02)00042-8

Brenguier F, Campillo M, Hadziioannou C, Shapiro NM, Nadeau RM, Larose E (2008) Postseismic relaxation along the San Andreas fault at parkfield from continuous seismological observations. Science 321:1478–1481. https://doi.org/10.1126/science.1160943

Brenguier F, Campillo M, Takeda T, Aoki Y, Shapiro NM, Briand X, Emoto K, Miyake H (2014) Mapping pressurized volcanic fluids from induced crustal seismic velocity drops. Science 345:80–82. https://doi.org/10.1126/science.1254073

Candela T, Brodsky EE, Marone C, Elsworth D (2015) Flow rate dictates permeability enhancement during fluid pressure oscillations in laboratory experiments. J Geophys Res Solid Earth 120:2037–2055. https://doi.org/10.1002/2014JB011511

Elkhoury JE, Brodsky EE, Agnew DC (2006) Seismic waves increase permeability. Nature 441:1135–1138. https://doi.org/10.1038/nature04798

Elkhoury JE, Niemeijer A, Brodsky EE, Marone C (2011) Laboratory observations of permeability enhancement by fluid pressure oscillation of in situ fractured rock. J Geophys Res 116:B02311. https://doi.org/10.1029/2010JB007759

Guyer RA, Johnson PA (2009) Nonlinear mesoscopic elasticity: the complex behavior of rocks, soil, and concrete. Wiley, Weinheim

Haupert S, Renaud G, Rivière J, Talmant M, Johnson PA, Laugier P (2011) High-accuracy acoustic detection of nonclassical component of material nonlinearity. J Acoust Soc Am 130:2654–2661. https://doi.org/10.1121/1.3641405

Hudson JA, Liu E, Crampin S (1996) The mechanical properties of materials with interconnected cracks and pores. Geophys J Int 124:105–112. https://doi.org/10.1111/j.1365-246X.1996.tb06355.x

Jin J, Rivière J, Ohara Y, Shokouhi P (2018) Dynamic acousto-elastic response of single fatigue cracks with different microstructural features: an experimental investigation. J Appl Phys. https://doi.org/10.1063/1.5036531

Jin J, Johnson P, Shokouhi P (2020) An integrated analytical and experimental study of contact acoustic nonlinearity at rough interfaces of fatigue cracks. J Mech Phys Solids 135:103769. https://doi.org/10.1016/j.jmps.2019.103769

Johnson P, Sutin A (2005) Slow dynamics and anomalous nonlinear fast dynamics in diverse solids. J Acoust Soc Am 117:124–130. https://doi.org/10.1121/1.1823351

Johnson PA, Zinszner B, Rasolofosaon PNJ (1996) Resonance and elastic nonlinear phenomena in rock. J Geophys Res Solid Earth 101:11553–11564. https://doi.org/10.1029/96JB00647

Johnson PA, Zinszner B, Rasolofosaon P, Cohen-Tenoudji F, Van Den Abeele K (2004) Dynamic measurements of the nonlinear elastic parameter α in rock under varying conditions. J Geophys Res Solid Earth. https://doi.org/10.1029/2002JB002038

Johnson PA, Bodin P, Gomberg J, Pearce F, Lawrence Z, Menq F-Y (2009) Inducing in situ, nonlinear soil response applying an active source. J Geophys Res 114:B05304. https://doi.org/10.1029/2008JB005832

Lawrence Z, Bodin P, Langston CA, Pearce F, Gomberg J, Johnson PA, Menq F-Y, Brackman T (2008) Induced dynamic nonlinear ground response at Garner Valley, California. Bull Seismol Soc Am 98:1412–1428. https://doi.org/10.1785/0120070124

Lott M, Remillieux MC, LeBas P-Y, Ulrich TJ, Garnier V, Payan C (2016) From local to global measurements of nonclassical nonlinear elastic effects in geomaterials. J Acoust Soc Am 140:EL231–EL235. https://doi.org/10.1121/1.4962373

Lubbe R (2005) A field and laboratory investigation of the compliance of fractured rock. University of Oxford, Oxford

Manogharan P, Wood C, Rivière J, Elsworth D, Marone C, Shokouhi P (2020) Elastodynamic nonlinear response of dry intact , fractured and saturated rock. Am. Rock Mech. Assoc. 54th U.S.

Niu F, Silver PG, Daley TM, Cheng X, Majer EL (2008) Preseismic velocity changes observed from active source monitoring at the Parkfield SAFOD drill site. Nature 454:204–208. https://doi.org/10.1038/nature07111

Ostrovsky LA, Johnson PA (2001) Nonlinear dynamics of rock: hysteretic behavior. Radiophys Quantum Electron 44:450–464. https://doi.org/10.1023/A:1017953331645

Pasqualini D, Heitmann K, TenCate JA, Habib S, Higdon D, Johnson PA (2007) Nonequilibrium and nonlinear dynamics in Berea and Fontainebleau sandstones: low-strain regime. J Geophys Res 112:B01204. https://doi.org/10.1029/2006JB004264

Pyrak-Nolte LJ, Nolte DD (2016) Approaching a universal scaling relationship between fracture stiffness and fluid flow. Nat Commun 7:10663. https://doi.org/10.1038/ncomms10663

Pyrak-Nolte LJ, Myer LR, Cook NGW (1990) Transmission of seismic waves across single natural fractures. J Geophys Res 95:8617. https://doi.org/10.1029/JB095iB06p08617

Remillieux MC, Guyer RA, Payan C, Ulrich TJ (2016) Decoupling nonclassical nonlinear behavior of elastic wave types. Phys Rev Lett 116:1–5. https://doi.org/10.1103/PhysRevLett.116.115501

Renaud G, Talmant M, Callé S, Defontaine M, Laugier P (2011) Nonlinear elastodynamics in micro-inhomogeneous solids observed by head-wave based dynamic acoustoelastic testing. J Acoust Soc Am 130:3583–3589. https://doi.org/10.1121/1.3652871

Renaud G, Le Bas P-Y, Johnson PA (2012) Revealing highly complex elastic nonlinear (anelastic) behavior of Earth materials applying a new probe: dynamic acoustoelastic testing. J Geophys Res Solid Earth. https://doi.org/10.1029/2011JB009127

Renaud G, Rivière J, Haupert S, Laugier P (2013a) Anisotropy of dynamic acoustoelasticity in limestone, influence of conditioning, and comparison with nonlinear resonance spectroscopy. J Acoust Soc Am 133:3706–3718. https://doi.org/10.1121/1.4802909

Renaud G, Rivière J, Le Bas P-Y, Johnson PA (2013b) Hysteretic nonlinear elasticity of Berea sandstone at low-vibrational strain

revealed by dynamic acousto-elastic testing. Geophys Res Lett 40:715–719. https://doi.org/10.1002/grl.50150

Renaud G, Rivière J, Larmat C, Rutledge JT, Lee RC, Guyer RA, Stokoe K, Johnson PA (2014) In situ characterization of shallow elastic nonlinear parameters with Dynamic Acoustoelastic Testing. J Geophys Res Solid Earth 119:6907–6923. https://doi.org/10.1002/2013JB010625

Renaud G, Talmant M, Marrelec G (2016) Microstrain-level measurement of third-order elastic constants applying dynamic acousto-elastic testing. J Appl Phys 120:135102. https://doi.org/10.1063/1.4963829

Rivière J, Renaud G, Guyer RA, Johnson PA (2013) Pump and probe waves in dynamic acousto-elasticity: comprehensive description and comparison with nonlinear elastic theories. J Appl Phys 114:054905. https://doi.org/10.1063/1.4816395

Rivière J, Remillieux MC, Ohara Y, Anderson BE, Haupert S, Ulrich TJ, Johnson PA (2014) Dynamic acousto-elasticity in a fatigue-cracked sample. J Nondestruct Eval 33:216–225. https://doi.org/10.1007/s10921-014-0225-0

Rivière J, Shokouhi P, Guyer RA, Johnson PA (2015) A set of measures for the systematic classification of the nonlinear elastic behavior of disparate rocks. J. Geophys. Res. Solid Earth 120:1587–1604. https://doi.org/10.1002/2014JB011718.Received

Rivière J, Pimienta L, Scuderi M, Candela T, Shokouhi P, Fortin J, Schubnel A, Marone C, Johnson PA (2016) Frequency, pressure, and strain dependence of nonlinear elasticity in Berea Sandstone. Geophys Res Lett 43:3226–3236. https://doi.org/10.1002/2016GL068061

Rutter EH, Mecklenburgh J (2017) Hydraulic conductivity of bedding-parallel cracks in shale as a function of shear and normal stress. Geol Soc Lond 454:67–84. https://doi.org/10.1144/SP454.9

Rutter EH, Mecklenburgh J (2018) Influence of normal and shear stress on the hydraulic transmissivity of thin cracks in a tight quartz sandstone, a granite, and a shale. J Geophys Res Solid Earth 123:1262–1285. https://doi.org/10.1002/2017JB014858

Samuelson J, Elsworth D, Marone C (2009) Shear-induced dilatancy of fluid-saturated faults: experiment and theory. J Geophys Res 114:B12404. https://doi.org/10.1029/2008JB006273

Sens-Schönfelder C, Eulenfeld T (2019) Probing the in situ elastic non-linearity of rocks with earth tides and seismic noise. Phys Rev Lett 122:138501. https://doi.org/10.1103/PhysRevLett.122.138501

Shokouhi P, Rivière J, Guyer RA, Johnson PA (2017a) Slow dynamics of consolidated granular systems: multi-scale relaxation. Appl Phys Lett. https://doi.org/10.1063/1.5010043

Shokouhi P, Rivière J, Lake CR, Le Bas PY, Ulrich TJ (2017b) Dynamic acousto-elastic testing of concrete with a coda-wave probe: comparison with standard linear and nonlinear ultrasonic techniques. Ultrasonics 81:59–65. https://doi.org/10.1016/j.ultras.2017.05.010

Shokouhi P, Jin J, Wood C, Rivière J, Madara B, Elsworth D, Marone C (2020) Dynamic stressing of naturally fractured rocks: on the relation between transient changes in permeability and elastic wave velocity. Geophys Res Lett 47:1–10. https://doi.org/10.1029/2019GL083557

TenCate JA (2011) Slow dynamics of earth materials: an experimental overview. Pure Appl Geophys 168:2211–2219. https://doi.org/10.1007/s00024-011-0268-4

Ten Cate JA, Shankland TJ (1996) Slow dynamics in the nonlinear elastic response of Berea sandstone. Geophys Res Lett 23:3019–3022. https://doi.org/10.1029/96gl02884

Van Den Abeele KE-A (2002) Influence of water saturation on the nonlinear elastic mesoscopic response in earth materials and the implications to the mechanism of nonlinearity. J Geophys Res 107:1–11. https://doi.org/10.1029/2001jb000368

Van Den Abeele K (2007) Multi-mode nonlinear resonance ultrasound spectroscopy for defect imaging: an analytical approach for the one-dimensional case. J Acoust Soc Am 122:73–90. https://doi.org/10.1121/1.2735807

Van Den Abeele KE-A, Carmeliet J, Ten Cate JA, Johnson PA (2000) Nonlinear elastic wave spectroscopy (NEWS) techniques to discern material damage, part II: single-mode nonlinear resonance acoustic spectroscopy. Res Nondestruct Eval 12:31–42. https://doi.org/10.1080/09349840009409647

Winkler KW, Liu X (1996) Measurements of third-order elastic constants in rocks. J Acoust Soc Am 100:1392–1398. https://doi.org/10.1121/1.415986

Winkler KW, McGowan L (2004) Nonlinear acoustoelastic constants of dry and saturated rocks. J Geophys Res Solid Earth 109:1–9. https://doi.org/10.1029/2004JB003262

Zinszner B, Johnson PA, Rasolofosaon PNJ (1997) Influence of change in physical state on elastic nonlinear response in rock: significance of effective pressure and water saturation. J Geophys Res Solid Earth 102:8105–8120. https://doi.org/10.1029/96JB03225